

Calibrating Dark Energy

Roland de Putter & Eric V. Linder

Lawrence Berkeley National Laboratory & University of California, Berkeley, CA 94720, USA

(Dated: August 1, 2008)

Exploring the diversity of dark energy dynamics, we discover a calibration relation, a uniform stretching of the amplitude of the equation of state time variation with scale factor. This defines homogeneous families of dark energy physics. The calibration factor has a close relation to the standard time variation parameter w_a , and we show that the new, calibrated w_a describes observables, i.e. distance and Hubble parameter as a function of redshift, typically to an accuracy level of 10^{-3} . We discuss implications for figures of merit for dark energy science programs.

I. INTRODUCTION

Understanding the nature of the dark energy accelerating the cosmic expansion is one of the premier questions in physics. The answer offers the possibility of deep insights into the nature of spacetime and gravity, extra dimensions, the quantum vacuum, and possibly the unification of gravitation and quantum physics. Precision mapping of the expansion history provides one path to characterizing the dark energy, in particular its equation of state and time variation.

Guidance from theory is useful to predict observable signatures for cosmological probes such as distance and Hubble parameter measurements, in particular what level of accuracy is required to distinguish between models. From a model one can predict distance-redshift relations etc. but the number of models is vast; one would like to identify model independent or at least generic characteristics of the dark energy. Indeed, such properties exist, as discussed in detail recently by [1], for classes of behavior in the early time evolution of dark energy, valid for $z \gtrsim 2$ when the dark energy does not strongly affect the background expansion.

In this article we seek to extend characterization of the dark energy properties in terms of the equation of state to the entire observable history. This requires a different approach, calibrating the evolution through a “stretch” relation between the amplitude of the time variation and the time variable or scale factor of the expansion. The calibration then provides a physical basis for a compact and highly accurate parametrization of the dark energy influence on observables.

In §II we examine several diverse models, looking for similarities and distinctions. We introduce the calibration in §III and discuss its relation to a standard parametrization of the equation of state. §IV examines the utility of the description and shows that it achieves robustness and accuracy at the 10^{-3} level, sufficient for next generation data. We discuss some implications for figures of merit of dark energy science programs in §V. Those readers wanting to get right to the results could start in the middle of §III.

II. DARK ENERGY DYNAMICS

By examining the behavior of a diversity of dark energy models representing different physical origins, we can explore common and distinct elements within 1) a model as the parameters vary, 2) a family of models with some related property, and 3) different classes of models. Families of models might consist of those with similar functional forms, e.g. polynomial potentials, while classes might be those with similar early time behaviors, e.g. thawing models or freezing models [2].

We choose five representative families ranging over different physics and different evolutionary histories. These are the pseudo-Nambu Goldstone boson (PNGB) model, or cosine potential, that thaws and moves away from an early cosmological constant state $w = -1$, the family of polynomial potentials, also thawing, the supergravity-inspired SUGRA model that has early tracking behavior and then moves toward the cosmological constant state (freezing behavior), the modified gravity model of DGP braneworld cosmology and its family of H^α modifications of the Friedmann equation, also with freezing behavior, and the Albrecht-Skordis or exponential times polynomial potential, whose history cannot be classified as purely thawing or freezing.

The dynamics is conveniently represented by the equation of state, or effective pressure to density ratio, w , and its variation $w' \equiv dw/d \ln a = \dot{w}/H$ where a is the expansion or scale factor. The Hubble parameter, or expansion rate, $H = \dot{a}/a$. We work in units where $8\pi G = 1$.

A. PNGB Model

Protected from radiative corrections by a shift symmetry, this model possesses technical naturalness and is characterized by a symmetry energy scale f [3]. The potential reads

$$V(\phi) = V_\star [1 + \cos(\phi/f)], \quad (1)$$

with V_\star setting the overall magnitude, hence related to the present dark energy density. The equation of state, and the dynamics in general, is governed by f and the initial field position ϕ_i . (It is convenient, as seen from the form of Eq. (1), to use ϕ_i/f instead of ϕ_i .)

One can scan over the parameter space of these three variables and examine the evolutionary behavior and viability as a dark energy model. Figure 1 shows a selection of trajectories in the w - w' plane. The time coordinate runs along these tracks, and can be thought of as the scale factor a or the dark energy density fraction of the total energy density, $\Omega_w(a)$. As we change V_\star or $\Omega_w = 1 - \Omega_m$, where Ω_m is the dimensionless present matter density, different points along a track for given f and ϕ_i/f correspond to the present. In fact, for some parameter values the dark energy never dominates and the density is restricted to $\Omega_w(a) < \Omega_{w,\max} < 1$. One can show that for fixed ϕ_i/f , then $\Omega_{w,\max} \propto f^2$, so models with symmetry energy scales much less than the Planck energy, $f \ll 1$, tend not to be viable.

Figure 1 shows a wide selection of trajectories that reach $\Omega_w = 0.72$ at the present. They fan out across the phase space, including ones that lie outside the conventional thawing region $3(1+w) > w' > 1+w$ (although these start along $w' = 3(1+w)$ at early times) [2]. The exceptions have $f \ll 1$, and are not generic in that for $f \ll 1$ we must fine tune ever more strictly the initial condition ϕ_i/f in order to achieve such a present density. Figure 2 plots the allowed values of ϕ_i/f , which decrease rapidly, roughly as $(\phi_i/f)_{\max} \sim e^{-1/f}$. For example, when $f = 0.1$, then the field must start exquisitely close to the top of the potential: rather than ϕ_i/f ranging freely over $[0, \pi]$, it is restricted to be less than 10^{-3} . For $f = 0.05$, this becomes $\phi_i/f < 10^{-7}$. Apart from unnaturalness, such values may run into physical problems such as a tachyonic instability [4, 5, 6].

In the future, the scalar field reaches the minimum of the potential and oscillates around it, giving an equation of state $w = 0$ (matter-like) when averaged over many oscillations. We discuss this further in comparison with the next model.

B. Linear Potential

The linear potential tilts a flat potential, so the field rolls – although it is frozen by the large Hubble friction at early times. The potential is given by

$$V(\phi) = V_i + (\phi - \phi_i) V', \quad (2)$$

where V' is the slope parameter, a constant [7, 8]. If the slope becomes too steep then the field never has time in its evolution to build up to appreciable energy density before the kinetic energy becomes substantial and $w > 0$, causing the fractional energy density relative to the matter density to decrease with scale factor. The evolutionary tracks for this model fan out in the phase space within the thawing region (some examples for this and other models appear in §IIF in Fig. 7).

Figure 3 shows the long time evolution of the PNGB vs. linear potential models, showing the similarity of the tracks at first, then the dramatic difference in the fate of the universe as the PNGB field oscillates, acting like

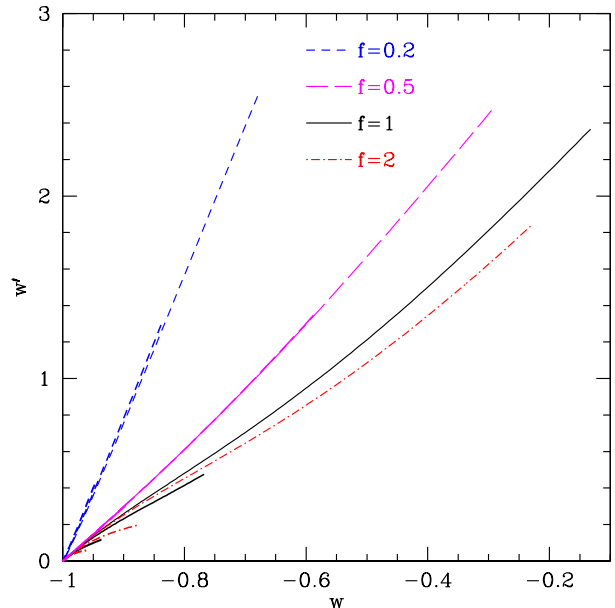


FIG. 1: PNGB models fan out through phase space as their parameters vary (though still mostly within the thawing region). At early times the models all start frozen at $(w, w') = (-1, 0)$ and thaw, with the scale factor increasing along each curve, although at different rates in each case. Here we end the tracks when $\Omega_w = 0.72$.

matter in a time averaged sense, and the linear potential field shoots away, leading to deceleration and a cosmic doomsday collapse.

We also consider the related family of polynomial potentials, $V \sim \phi^n$ with $n = 2, 4$. These are also thawing models although their future behavior asymptotes to oscillation about a zero potential minimum. Hence they do not runaway to negative potential and a rapid, doomsday collapse. The equation of state during the oscillatory phase time averages to $w = (n - 2)/(n + 2)$ [9].

C. SUGRA Model

Tracking models have an early time attractor behavior that allows a large variety of initial conditions to give the same evolution in the matter dominated era, ameliorating fine tuning of initial conditions [10]. One example is the family of inverse power law potentials [11]. Including Planck scale corrections motivated by supergravity theory changes the potential to [12]

$$V(\phi) = V_\star \phi^{-n} e^{\phi^2/2}. \quad (3)$$

This has a local nonzero minimum, or cosmological constant. The equation of state behavior is governed by the power law index n .

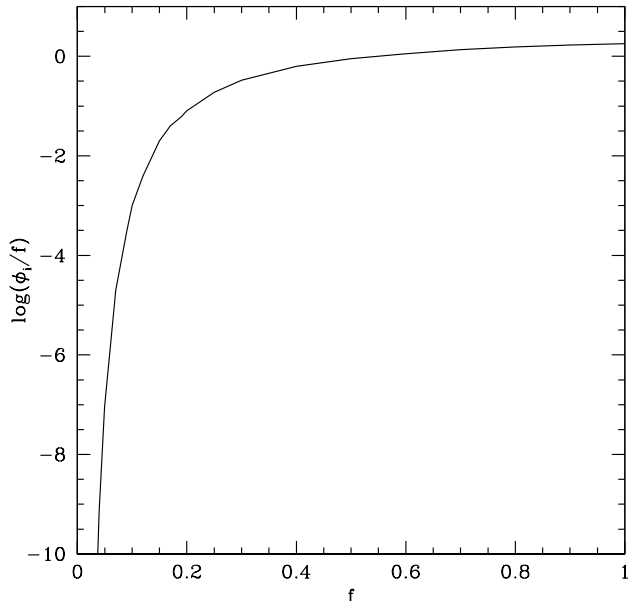


FIG. 2: To achieve dark energy domination in the PNGB model before the field relaxes to its minimum, the initial field value ϕ_i must be small enough to give a long period of cosmological constant-like, or frozen, behavior. For very steep potentials, i.e. low symmetry energy breaking scales f , the field must initially be extremely finely balanced near the top of the potential, with the curve showing the maximum ϕ_i/f allowed to achieve $\Omega_w \geq 0.72$ at some point in the evolution.

Although the exponential factor has no effect on the attractor phase, it does permit a more rapid evolution after the field leaves that trajectory, moving the equation of state closer to $w = -1$. Since the dark energy has $w = -2/(2+n)$ while on the attractor trajectory, one requires $n \ll 1$ in the inverse power law model to accord with observations; this is somewhat eased for the SUGRA model. Today the field properties can cover a wide swath within the freezing region $0.2w(1+w) < w' < 3w(1+w)$.

D. Braneworld Gravity Model

Even dark energy theories that do not involve scalar fields can be viewed in terms of effective dynamics, where the equation of state is defined in terms of the Hubble parameter $H(a)$ and its modified Friedmann equation:

$$w_{\text{eff}} = -1 - \frac{1}{3} \frac{d \ln \delta H^2}{d \ln a}, \quad (4)$$

where $\delta H^2 = H^2/H_0^2 - \Omega_m a^{-3}$. One example involving very different physics from scalar fields is the extension of gravity theory through extra dimensions. This can lead to a modified Friedmann equation and effective equation

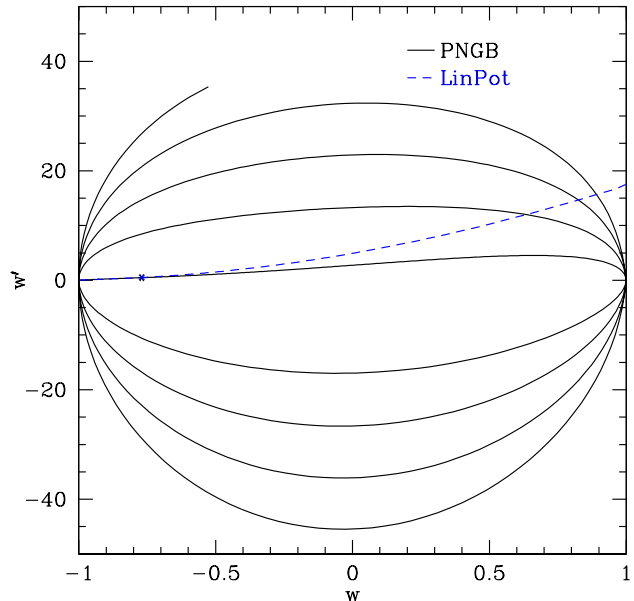


FIG. 3: Long term evolutions of PNGB and linear potential models have distinct implications for the fate of the universe, both different from the cosmological constant case. The PNGB field oscillates while the linear potential rolls to negative infinity. Today the models shown have $w_0 = -0.77$, with $w'_0 = 0.47, 0.52$ respectively. At $a = 2$, the PNGB model is still on the innermost track, with $w = 0.11$ (the curve end is at $a = 6.6$), while the linear potential is off the plot, on the way to collapse.

of state [13, 14]

$$H^2 = \rho_m(a)/3 + (1 - \Omega_m) H_0^2 (H/H_0)^\alpha, \quad (5)$$

$$w = - \left[1 + \frac{\alpha}{2 - \alpha} \Omega_m(a) \right]^{-1}, \quad (6)$$

where ρ_m is the physical matter density and α is a parameter depending on boundary conditions between our four dimensional universe and the higher dimensional bulk volume. The best motivated model in this family is DGP braneworld gravity, corresponding to $\alpha = 1$ [15, 16]. At early times the effective potential looks like an inverse power law [1], with index $n = 2\alpha/(2 - \alpha)$, and so has tracking behavior. At late times the field rolls asymptotically to a halt at a finite value of both the field and potential, acting as a cosmological constant. Indeed the trajectories lie within the freezing region.

E. Albrecht-Skordis Model

A scalar field potential with greater complexity is the Albrecht-Skordis [17], or exponential with polynomial prefactor, potential, motivated by string theory. This

has the form

$$V(\psi) = V_0 [\chi(\psi - \beta)^2 + \delta] e^{-\lambda\psi}, \quad (7)$$

in the notation of [18], with a more compact but equivalent notation being

$$V(\phi) = V_\star (1 + A\phi^2) e^{-\lambda\phi}, \quad (8)$$

where we shift to $\phi = \psi - \beta$, showing that only three parameters enter: V_\star , related to the dark energy density today, λ , and A . Away from $\phi \approx 0$ this behaves like an exponential potential, a classic tracker, so the initial conditions are not very important [19]. Near $\phi = 0$, the potential has a false minimum, so a field rolling through this region can have complicated dynamics, and indeed be trapped and oscillate about the nonzero potential minimum, eventually relaxing to a cosmological constant.

Figure 4 show trajectories for different parameter values, illustrating the wide variety of possible behaviors. In addition, Fig. 5 plots the equation of state $w(a)$ so one has another view of the damped, oscillatory evolution. Note that while the field sees an exponential potential, away from the false minimum, it exhibits not only tracking but tracing behavior – the dark energy equation of state is equal to the background, e.g. matter dominated, equation of state w_b . This means that the dark energy density is then a constant fraction of the background density, given by $\Omega_{w,\text{trace}} = 3(1+w_b)/\lambda^2$ [20, 21]. So as not to violate primordial nucleosynthesis or cosmic microwave background constraints, this requires the contribution to be no more than a few percent. We show the dynamics for two cases, the first using the parameter values in [18], corresponding to $\lambda = 3.4$ and $A = 106.7$, which has an early dark energy fraction $\Omega_e = 0.26$ during matter domination ($\Omega_e = 0.35$ during radiation domination), and the second using $\lambda = 10$, keeping A the same, giving $\Omega_e = 0.03$ (0.04) during matter (radiation) domination, close to the upper limit allowed [22, 23].

For values of λ allowed by nucleosynthesis and CMB limits, $\lambda \geq 10$, the oscillations are absent or negligible. One can show that the amplitude of the oscillations depends predominantly on the ratio λ^2/A (e.g. define $\varphi = \lambda\phi$ and the potential only explicitly contains the parameter combination λ^2/A). If this combination exceeds one, then there is no minimum but merely a slight local lessening of the exponential slope, and hence no oscillations. The amplitude increases as λ^2/A approaches zero. However, since $\lambda \geq 10$, small values of λ^2/A require $A \gtrsim 1000$, seemingly unnatural. Furthermore, the period of the oscillations is given by the effective mass and is inversely proportional to λ for fixed λ^2/A , and so for allowed λ the oscillations will be negligible for $z \lesssim 3$. These behaviors are illustrated in Fig. 6.

F. Cross Comparison

To compare the behaviors of different families, we plot selected representatives in Fig. 7. Varying the param-

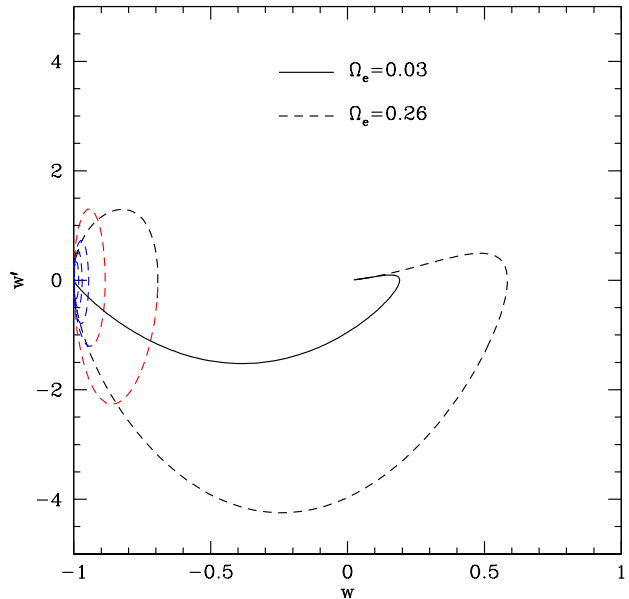


FIG. 4: Albrecht-Skordis model acts like a tracer at early times, with a constant energy density fraction Ω_e and $w = 0$ in the matter dominated era, before oscillating around the nonzero minimum of the potential. We change the line thicknesses (and colors) at $z = 2, 1$, and 0 . The oscillations are invisible for more viable $\Omega_e = 0.03$ case.

eters within each model, as well as considering different models, spreads the evolution over regions of the w - w' phase space. Generally we see both similarities and distinctions between models and between families. One must also take into account the time coordinate along the curves, so that crossing of trajectories does not mean they have identical properties at any one moment. We plot the trajectories up to when the dark energy density is $\Omega_w = 0.72$.

We could extend the curves into the future, as was done in Figs. 3 and 4. The ϕ^4 potential will eventually settle at $w = 1/3$, acting as radiation, as discussed in §II B, after oscillating around the minimum. Note that the SUGRA, DGP/ H^α , and Albrecht-Skordis models all have nonzero minima, i.e. hidden cosmological constants, so they settle to $w = -1$. The SUGRA field does not oscillate around the minimum because it approaches it with low kinetic energy, freezing to the cosmological constant state; the H^α family has only an asymptotic minimum, also approached by freezing.

As an alternative to showing the evolution of varied models at all times, we can take a slice at a particularly time, say when $\Omega_w = 0.72$, and construct phase space curves where the parameters of a potential vary along the curve. This can clear the illusion of overlap in behavior and provides an intermediate step toward the calibration in the next section.

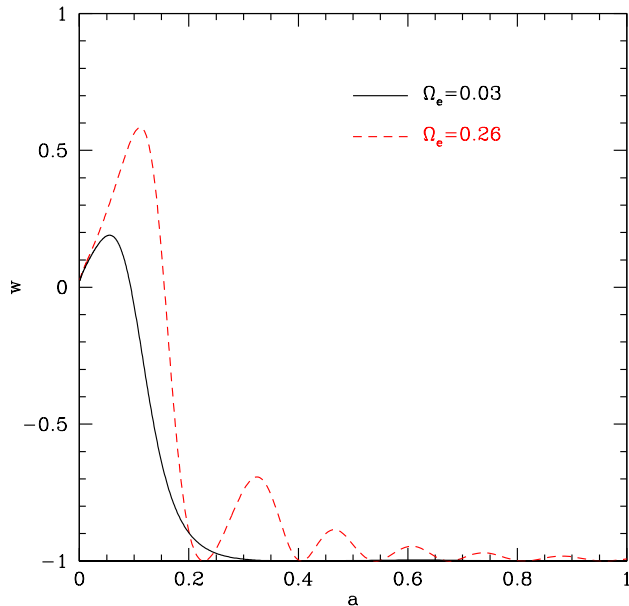


FIG. 5: Equation of state $w(a)$ shows an alternate view of the evolution in Fig. 4. Note that for model parameters that do not violate early matter domination, the behavior relaxes swiftly to a cosmological constant, as shown by the solid, black curve.

Figure 8 gives an example of this for the PNGB model, where the parameter running along the curve is the initial field position ϕ_i/f . That is, every point along any curve has $\Omega_w = 0.72$ today, but corresponds to a different set of parameters for the potential and a different evolutionary behavior. This illustrates that different symmetry energy scales f define distinct paths to achieving a given dark energy density. (Of course not all of these are viable, with large values of ϕ_i/f along each curve corresponding to w far from -1 , and small values of f suffering from the extreme fine tuning problem discussed in §II A.) However, by evaluating the equation of state and its time variation at a single time, we lose all dynamical information. In the next section we combine the advantages of the parameter scan with those of the evolutionary trajectories.

III. STRETCHING DARK ENERGY

To keep the dynamics central, we want to preserve in some way the temporal information, i.e. the field evolving from its high redshift state along a trajectory describing the equation of state and its time variation. However, we are free to rescale the time coordinate and define a time variation other than $w' = dw/d\ln a$. In particular, we can ask whether there is a global transformation that in some way calibrates the dark energy characteristics. We call this the evolutionary stretch factor.

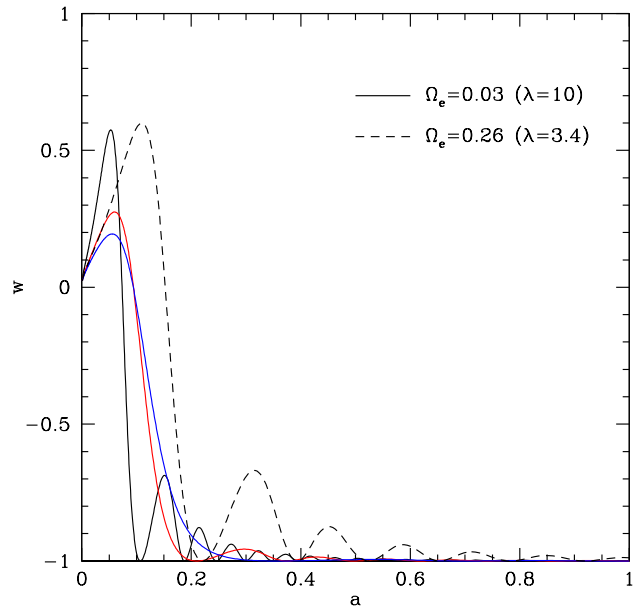


FIG. 6: The amplitude of oscillations in the equation of state is governed by λ^2/A and the period goes as λ^{-1} (for fixed λ^2/A). The figure shows the equation of state history for $\lambda = 10$ ($\Omega_e = 0.03$ during matter domination) as solid curves, for $\lambda^2/A = 0.1, 0.5, 0.9$, from highest peak to lowest, and for $\lambda = 3.4$ ($\Omega_e = 0.26$), with $\lambda^2/A = 0.1$, as a dashed curve. For appreciable oscillations λ^2/A must approach zero, but for allowed (large) values of λ any oscillations damp away for $z \lesssim 3$.

Stretching the time variation by different amounts at different times effectively introduces additional evolution beyond the scalar field behavior, so we consider a constant stretch factor, a simple renormalization. That is, we take $w'(a) \rightarrow w'(a)/a_*$. Now, since realistic observations cannot map out the detail of the equation of state function, we seek to condense the information on the evolution to a set that is robustly constrained by data. Overcompression loses important physical properties while undercompression leads to uninformatively large uncertainties. In the next section we will test the full stretch prescription to ensure that neither case occurs. To begin with, consider evaluating our new time variation quantity at a particular scale factor; furthermore, to keep the number of parameters in the stretch prescription to a minimum, we choose this scale factor to be the same as the stretch factor a_* . That is, the procedure can be viewed illustratively as

$$w'(a) \rightarrow \frac{w'(a)}{a_*} \rightarrow \frac{w'(a_*)}{a_*}. \quad (9)$$

For evaluating the value of the equation of state function itself, $w(a)$, we also avoid choosing an arbitrary scale factor. This leaves us with two choices: either a_* or the

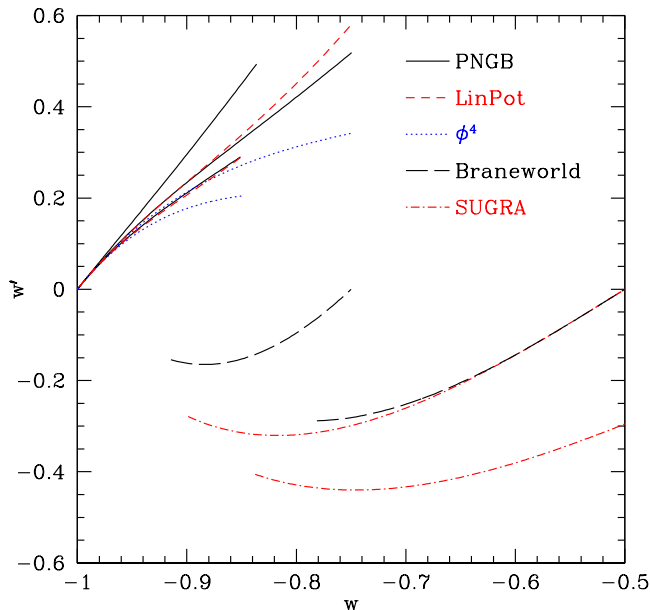


FIG. 7: Representative models considered in this section are plotted for various parameter values in the w - w' phase space. Solid, black curves are PNGB, short-dashed, red curves are for the linear potential, dotted, blue curves are for ϕ^4 , long-dashed, black curves for the braneworld model ($\alpha = 1$ DGP and $\alpha = 0.5$), and dot-dashed, red curves for SUGRA.

present epoch, $a = 1$. If we choose a_* , then this procedure merely chooses a single point along the evolutionary trajectory, losing much of the global information. Thus we adopt $w_0 = w(a = 1)$ and examine the dark energy characteristics in the plane of the two parameters, w_0 and $w'(a_*)/a_*$ ($= dw/da(a_*)$), to see if there is indeed a normalizing relation for the time evolution.

Figure 9 shows clearly that this prescription calibrates the evolution of the PNGB model. Instead of the fan of trajectories spreading through the w - w' phase space, as in Fig. 8, we now have a tightly calibrated, one parameter relation in the w_0 vs. $w'(a_*)/a_*$ plane. Despite scanning over the model space of f and ϕ_i/f , this stripe is narrow and well defined. Points within the stripe represent individual realizations of the PNGB model with choices of the symmetry energy scale ranging over the physically reasonable range $f \in [0.2, 5]$ and initial field position covering from 0 to the maximum value that allows $\Omega_w \approx 0.7$.

This tight calibration spreads little if we vary the present dark energy density as well as the potential parameters themselves. Allowing Ω_w today to range over 0.69-0.75 gives the slightly wider, lightly shaded region.

Calibration succeeds for the other dark energy models considered as well, covering a wide range of physical origins. Indeed, all the thawing models are closely related, nearly forming a single family under the calibration. The similarities extend to defining a single stretch parameter

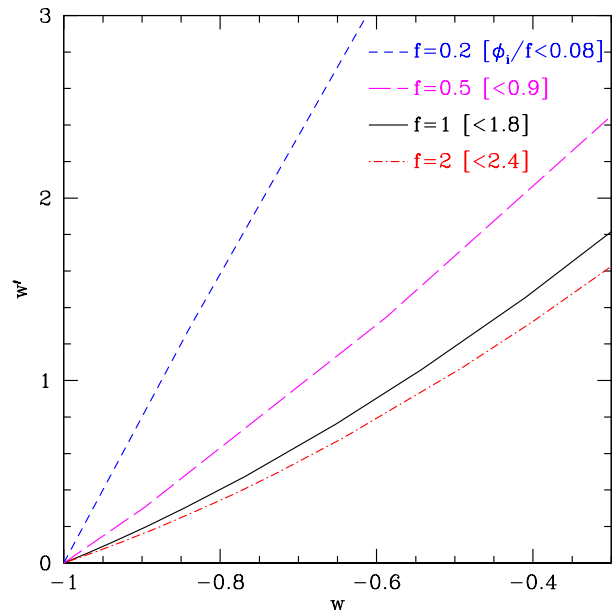


FIG. 8: These curves for the PNGB model correspond to a scan over the potential parameter space to find those values where $\Omega_w = 0.72$. Each curve is for a different energy scale f , with the parameter ϕ_i/f running along each curve, from zero at $w = -1$ to a maximum possible value shown in brackets.

$a_* = 0.8$ for the entire thawing class. Freezing fields also can be calibrated, with a uniform stretch parameter $a_* = 0.85$, though the families stay more distinct within the freezing class. Figure 10 shows the tight relations of the different dark energy models, in strong contrast with the “fan” nature of Fig. 7.

From the form of the stretch calibrated time variation, $w'(a_*)/a_*$, we can recognize this as nearly identical to w_a , the dark energy variable in standard use, defined by [24] as $w_a = -w'(a_*)/a_*$ to fit the equation of state function by $w(a) = w_0 + w_a^{(w)}(1 - a)$. The superscript w indicates that the value of a_* was chosen to fit $w(a)$. Here, however, we defined the equivalent of w_a to calibrate dark energy families. This resulted in $a_* = 0.8$ for the thawing class and $a_* = 0.85$ for the freezing class. An interesting further implication is that the “new” form

$$w(a) = w_0 - \frac{w'(a_*)}{a_*}(1 - a) = w_0 + w_a^{(d)}(1 - a) \quad (10)$$

has excellent accuracy when fitting the observables of distance and Hubble parameter, as we discuss next.

IV. OBSERVING DARK ENERGY

While the form (10) was just shown useful in interpretation of dark energy theory, we should also investigate its utility for interpreting dark energy observations.

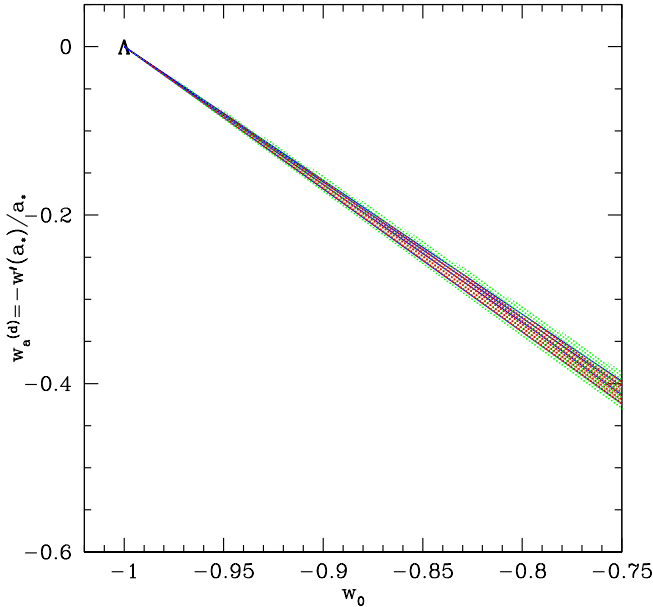


FIG. 9: Defining a new time variation variable $w_a^{(d)}$ from w' calibrates the PNGB model into a tight locus; compare the spread in Fig. 8. Solid lines are for fixed f parameter, the shading shows the range of behaviors for $f \in [0.2, 5]$. The lighter shading shows the effect of also scanning over $\Omega_m = 0.25\text{--}0.31$.

Three related, but slightly different, physical bases exist for using the form $w(a) = w_0 + w_a(1 - a)$ to characterize dark energy: this can be interpreted as 1) a fitting formula to the equation of state, 2) a calibration relation for families of dynamics in the w - w' plane, or 3) a fitting formula for observables such as distances and the Hubble expansion rate. The last two in particular are closely related and give similar results; indeed, when models do not deviate greatly from cosmological constant behavior the two approaches are almost identical.

We now explore the accuracy of the form (10) in fitting the exact distance-redshift and Hubble parameter-redshift relations for the diverse dark energy models discussed in §II.

Table I summarizes the accuracies on d and H for a diverse range of models. These are generally good to the 10^{-3} level. Models closer to Λ would have better fits than shown here; models further from Λ are not favored by current data. For simplicity we henceforth denote the calibrated fit parameter simply as w_a .

We could push the accuracy even further by minimizing the deviation not globally, over the entire range $a \in [0, 1]$, but over a particular epoch, say $a \in [0.5, 1]$. However, we retain the global fit in general. Also, we have not taken advantage of the degree of freedom of w_0 , which could improve the fits. We emphasize that the stretch factor is a function of the dark energy physics

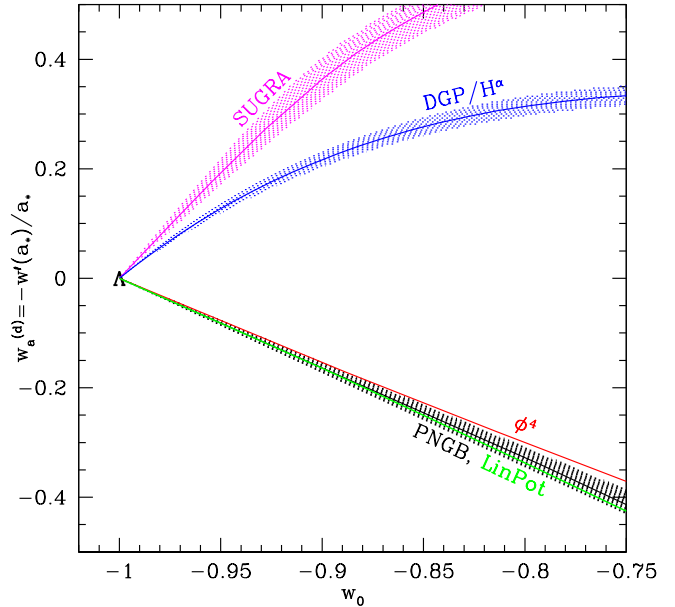


FIG. 10: In terms of the calibrated dark energy parameters w_0 and $w_a^{(d)}$, models and families lie in tightly homogeneous regions, in comparison to Fig. 7, showing the same models before calibration. We here vary over all parameters in the potentials. Shading shows the effect of scanning over ± 0.03 in Ω_m (we omit the shading for ϕ^4 and linear potential models to minimize confusion; the width would be about half that shown for PNGB). Thawing models, despite their differences in w - w' , are nearly identical once calibrated. Distinctions from freezing models, and between freezing models, become highlighted with calibration.

and not dependent on the experiment, priors, etc. (in distinction from a pivot redshift or pivot equation of state value).

Note that the results from this prescription also answer the important question of whether the calibration procedure preserves the information faithfully to the precision level of the data, or over- or under-compresses the model characteristics. A one parameter approach such as a constant value of w would have errors of order 1–2% in distance and up to 3% in Hubble parameter for the models we considered. This is insufficient for forthcoming observations. Conversely, since the two calibrated parameters of w_0 and w_a map the observables to better accuracy than expected from next generation data, these two parameters suffice and the data precision does not call for further equation of state parameters.

This is not to say that some models could not exist where a third parameter carries information, but such models may not be generic or natural; the wide range of models considered here has no use for one. If we reach the stage of probing the cosmic expansion history below the 10^{-3} precision level, we should revisit the question of a further calibration parameter.

Model	$\delta d/d$	$\delta H/H$
PNGB ($w_0 = -0.85$)	0.05%	0.1%
PNGB ($w_0 = -0.75$)	0.1%	0.2%
Linear Pot. ($w_0 = -0.85$)	0.05%	0.1%
Linear Pot. ($w_0 = -0.75$)	0.1%	0.3%
ϕ^4 ($w_0 = -0.85$)	0.01%	0.04%
ϕ^4 ($w_0 = -0.75$)	0.02%	0.06%
Braneworld ($w_0 = -0.78$)	0.03%	0.07%
SUGRA ($n = 2$)	0.1%	0.3%
SUGRA ($n = 11$)	0.1%	0.3%
Albrecht-Skordis ($\Omega_e = 0.03$)	0.01%	0.02%
Albrecht-Skordis ($\Omega_e = 0.26$)	0.1%	0.4%

TABLE I: Accuracy of w_0 - w_a in fitting the exact distances and Hubble parameters for various dark energy models. These numbers represent global fits over all redshifts (except for the last three cases, where the fit covers $z = 0$ -3, due to early dark energy: see §V). Better fits can be found over finite redshift ranges.

Finally, this prescription is meant to help us find our way through the dark forest [25] of models of cosmic acceleration, making accurate, more or less model independent assessments. Once precision data exist, they should be analyzed for every model of interest and within every applicable fit technique, parametric and nonparametric. We have seen that until we reach that point w_0 - w_a serves as a robust indicator and guide for predicting and comparing cosmological probe information.

V. FIGURES OF MERIT

The accuracy of the w_0 and w_a form, defined in the manner discussed here, for characterization of observable properties of dark energy is at a level of order 10^{-3} , sufficient for next generation experiments. The calibration into tight families of equation of state properties, as seen in Fig. 7, suggests that not all combinations of w_0 and w_a are of equal insight. For example, one might distinguish models in the thawing class from the cosmological constant and from each other by constraining the combination varying exactly along the calibrated curve.

Since this curve is nearly straight, we can characterize it by slope m_t , and define a new variable

$$w_{\parallel}^t = w_0 + m_t w_a, \quad (11)$$

where the derivative with respect to this parameter runs parallel to the calibrated curve. Hence, determining w_{\parallel}^t localizes the behavior and distinguishes the specific dark energy characteristics. The narrowness of the calibrated region means that it is not so useful within thawing models to constrain the direction perpendicular to the curve.

One can define a similar variable for the freezing class, although here the families are more spread out, so the

slope is more of an average than a well defined value,

$$w_{\parallel}^f = w_0 + m_f w_a. \quad (12)$$

Values of $m_t = -1.75$ and $m_f = 3.5$ are reasonable choices. Note that the combinations w_{\parallel}^f and w_{\parallel}^t are not orthogonal, so the variable defined for each class does have utility in constraining the other class as well. For example, along the PNGB curve of Fig. 10 the parameter w_{\parallel}^t runs from -1 to 0 , while w_{\parallel}^f goes from -1 to -2.2 ; along the SUGRA curve $w_{\parallel}^t = -1$ to -1.7 while $w_{\parallel}^f = -1$ to $+0.9$. This shows that each parameter, while optimized for a given physics question, does carry information on the other class.

Thus, knowledge of either parameter w_{\parallel}^t or w_{\parallel}^f answers the key questions of distinction from a cosmological constant, distinction between models, and to an extent distinction between classes. Constraining both parameters tightens the distinguishing ability, especially between classes, and provides a crucial crosscheck of the framework.

It does not seem natural or effective to combine the uncertainties in estimating these variables from observations into a single number, e.g. $\sigma(w_{\parallel}^t) \times \sigma(w_{\parallel}^f)$, since they represent very different physics. Moreover, further investigation is needed into the optimum values for m_f , m_t and other issues before defining ultimate figures of merit, if this is even possible. However, the tightness of the calibration does imply that some combinations of w_0 and w_a will provide insight into the nature of dark energy. Therefore, knowledge of the uncertainties $\sigma(w_0)$ and $\sigma(w_a)$ and their covariance are the main ingredients for a variety of future figures of merit that might be developed.

Finally, we note that the accuracy of the w_0 - w_a form does start to degrade to the 10^{-2} level as dark energy becomes increasingly important in the early universe around $z \gtrsim 10^3$, upsetting standard matter domination. See, for example, the last three models in Table I, where the dark energy equations of state at recombination are $w \approx -0.15, 0, 0$, respectively. It could be useful to treat such early dark energy models as a separate class, and include constraint on the dark energy density Ω_e at recombination (which can best be done through growth probes) as another desideratum for a dark energy science program.

VI. CONCLUSIONS

Having investigated a diverse group of dark energy models to explain the acceleration of the cosmic expansion, we find a homogeneous “stretch” relation that calibrates the time variation behavior into tight families. This stretch factor is closely related to the standard time variation measure w_a , and we verify that the equation of state form $w(a) = w_0 + w_a(1 - a)$, with w_a now treated

as a fit parameter to observables, delivers fractional accuracy at the 10^{-3} level.

Such accuracy is sufficient for next generation data and the w_0 - w_a form can be viewed as an appropriate compression of the expansion history information that can be extracted from such observations. That is, this form neither overcompresses (loses important information) nor undercompresses (lacks additional leverage). This indicates there is no need nor generic benefit for going to a third parameter. Note that [26] saw similar compression and tight relations within a principal component analysis relying on many modes.

To gain insight into the nature of dark energy, particular combinations of w_0 - w_a may have enhanced leverage and hence merit, separating the cosmological constant from the thawing class, each from the freezing class, and possibly zeroing in on specific models within a class.

The calibration, and its robustness and accuracy in accounting for the observable relations, offers a well-defined method for assessing the next generation dark energy science program. Interpretation of those observations should offer promising insights into the physics of the accelerating universe.

Acknowledgments

We thank Andy Albrecht and Michael Barnard for helpful discussions. This work has been supported in part by the Director, Office of Science, Office of High Energy Physics, of the U.S. Department of Energy under Contract No. DE-AC02-05CH11231.

-
- [1] R.N. Cahn, R. de Putter, E.V. Linder, arXiv:0807.1346
 - [2] R.R. Caldwell & E.V. Linder 2005, Phys. Rev. Lett. 95, 141301
 - [3] J.A. Frieman, C.T. Hill, A. Stebbins, I. Waga 1995, Phys. Rev. Lett. 75, 2077
 - [4] S. Tsujikawa & T. Torii 2000, Phys. Rev. D 62, 043505
 - [5] D. Cormier & R. Holman 2000, Phys. Rev. Lett. 84, 5936
 - [6] N. Kaloper & L. Sorbo 2006, JCAP 0604, 007
 - [7] A. Linde 1987, in *Three Hundred Years of Gravitation*, ed. S W Hawking & W Israel (Cambridge: Cambridge U. Press), p. 604
 - [8] S. Weinberg 2008, *Cosmology* (Oxford U. Press)
 - [9] M.S. Turner 1983, Phys. Rev. D 28, 1243
 - [10] I. Zlatev, L. Wang, P.J. Steinhardt 1999, Phys. Rev. Lett. 82, 896
 - [11] B. Ratra & P.J.E. Peebles 1988, Phys. Rev. D 37, 3406
 - [12] P. Brax & J. Martin 1999, Phys. Lett. B 468, 40
 - [13] G. Dvali & M.S. Turner 2003, arXiv:astro-ph/0301510
 - [14] P. Gondolo & K. Freese 2003, Phys. Rev. D 68, 063509
 - [15] G. Dvali, G. Gabadadze, M. Porrati 2000, Phys. Lett. B 485, 208
 - [16] C. Deffayet, G. Dvali, G. Gabadadze 2002, Phys. Rev. D 65, 044023
 - [17] A. Albrecht & C. Skordis 2000, Phys. Rev. Lett. 84, 2076
 - [18] M. Barnard, A. Abrahamse, A. Albrecht, B. Bozek, M. Yashar 2008, Phys. Rev. D 77, 103502
 - [19] C. Wetterich 1988, Nucl. Phys. B 302, 668
 - [20] P.G. Ferreira, M. Joyce 1998, Phys. Rev. D 58, 023503
 - [21] E.J. Copeland, A.R. Liddle, D. Wands 1998, Phys. Rev. D 57 4686
 - [22] M. Doran, G. Robber, C. Wetterich 2007, Phys. Rev. D 75, 023003
 - [23] R. Bean, S.H. Hansen, A. Melchiorri 2001, Phys. Rev. D 64, 103508
 - [24] E.V. Linder 2003, Phys. Rev. Lett. 90, 091301
 - [25] D. Alighieri 1321, *Inferno*, Canto I, 2
 - [26] M. Barnard, A. Abrahamse, A. Albrecht, B. Bozek, M. Yashar, arXiv:0804.0413